Applied Catalysis B: Environmental 86 (2009) 63–68

Contents lists available at ScienceDirect

Applied Catalysis B: Environmental

journal homepage: www.elsevier.com/locate/apcatb

Titanium-doped nanocomposite of Al_2O_3 and ZrO_2–TiO_2 as a support with high sulfur durability for NO_x storage-reduction catalyst

Haruo Imagawa *, Toshiyuki Tanaka, Naoki Takahashi, Shin'ichi Matsunaga, Akihiko Suda, Hirofumi Shinjoh

Toyota Central Research and Development Labs, Inc., 41-1 Yokomichi, Nagakute, Nagakute-cho, Aichi 480-1192, Japan

ARTICLE INFO

Article history:
Received 18 March 2008
Received in revised form 7 June 2008
Accepted 22 July 2008
Available online 30 July 2008

Keywords:
Titanium-doped
Nanocomposite
Solid solution
Sulfur durability
NO_x storage-reduction catalyst

ABSTRACT

A nanocomposite of Al_2O_3 and a ZrO_2–TiO_2 solid solution (AZT) doped with Ti (Ti–AZT) was synthesized as a support for a NO_x storage-reduction (NSR) catalyst in order to achieve sulfur durability. Ti–AZT maintained the original structure of AZT after the Ti doping step and exhibited lower basicity. Energy dispersive X-ray spectroscopy revealed that the Ti concentration on the Al_2O_3 particles was more than 10 at.% on average for a sample containing 3.3 at.% of doped titanium. Doped titanium was homogeneously distributed on the surface without the formation of discrete TiO_2 particles. SO_2-temperature programmed desorption at less than 823 K indicated that the catalyst containing Ti–AZT had larger sulfur desorption than that containing AZT. After sulfur aging tests, the Ti–AZT catalyst provided a large amount of NO_x storage. The improved sulfur durability in the NSR catalyst resulted from the presence of TiO_2 as a Al_2O_3–TiO_2 solid solution in Ti–AZT.

1. Introduction

The lean-burn engine system is one of the most attractive methods to reduce the emission of carbon dioxide (CO_2) from vehicles, with regard to global environmental practices. However, in this system, conventional three-way catalysts cannot reduce nitrogen oxides (NO_x) into nitrogen (N_2) under lean conditions, because excess oxygen is present in the exhaust gases. Therefore, a number of challenging catalyst systems have been developed to reduce NO_x in lean systems [1–3].

The NO_x storage-reduction catalyst (NSR catalyst) has been proposed as one of the promising methods for the purification of NO_x from lean-burn engines [4,5]. The NSR catalyst has the following mechanism for NO_x storage and reduction reactions [6]. Firstly, during the lean condition, excess NO_x is oxidized to NO_2 on precious metal catalysts and stored in the form of nitrate within the storage materials. Secondly, when the engine is switched to operate on a rich air–fuel ratio, the nitrates stored in the storage material are reduced to N_2 by hydrogen (H_2), carbon monoxide (CO), and hydrocarbons (HC).

The NSR catalyst has two main technical problems: sulfur poisoning and thermal deterioration. Sulfur poisoning is caused by the presence of sulfur dioxide (SO_2) in the gas exhaust. SO_2 adsorbs onto the catalysts and then reacts with the storage materials. Finally, the catalysts cannot store NO_x, due to the formation of sulfates. In an attempt to solve this problem, the effect of sulfur on storage materials has been well studied [7–11]. Recent studies on sulfur durability in catalysts have reported that TiO_2 in support materials provides high tolerance against sulfur poisoning, due to its high acidity/low basicity [6,7,12–14]. TiO_2 is often contained in the ZrO_2–TiO_2 solid solution to prevent the solid-phase reaction of the NO_x storage materials with TiO_2 under heating [6,13]. The properties of ZrO_2–TiO_2 have also been well demonstrated in terms of weak basicity [6,14].

Thermal deterioration of the catalyst occurs due to the aggregation of the support particles and precious metals [15], in addition to the solid-phase reaction of the NO_x storage materials [16,17]. Therefore, Al_2O_3 is added to the support, because of its excellent thermal stability. Recently, we developed a novel nanocomposite of Al_2O_3 and ZrO_2–TiO_2 (AZT) as a support [18]. In this nanocomposite, Al_2O_3 primary particles and ZrO_2–TiO_2 primary particles coexist within the same secondary particle. AZT has been shown to inhibit the thermal aggregation of ZrO_2–TiO_2, because Al_2O_3 acts as a diffusion barrier to ZrO_2–TiO_2 particles in the form of secondary particles (Fig. 1). Particle growth of not only ZrO_2–TiO_2, but also of precious metals on the supports is prevented, and high NSR performance is achieved. Furthermore, AZT has been found to have low basicity, which is expected, due to

* Corresponding author. Tel.: +81 561 71 7226; fax: +81 561 63 5743.
E-mail address: e1152@mosk.tytlabs.co.jp (H. Imagawa).

0926-3373/$ – see front matter © 2008 Elsevier B.V. All rights reserved.
doi:10.1016/j.apcatb.2008.07.019

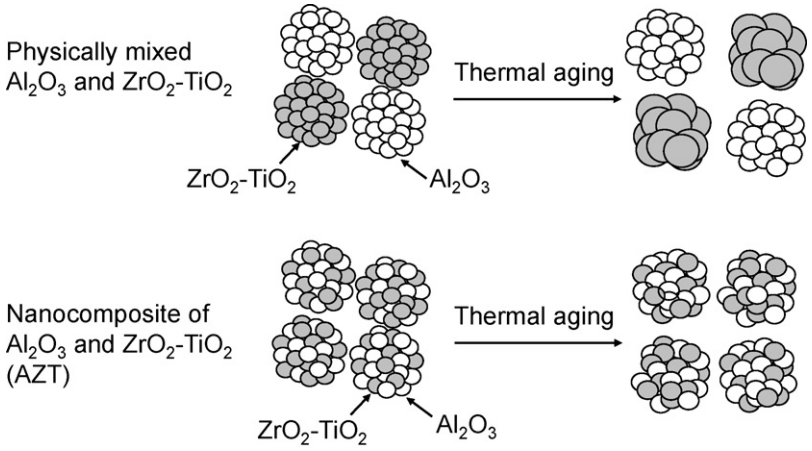

Fig. 1. Concept chart of AZT.

the presence of the small amount of TiO_2 in Al_2O_3. Therefore, the NSR catalyst containing AZT as a support is expected to exhibit not only excellent thermal stability, but also higher sulfur durability, because all of the particles contain TiO_2. It is also postulated that the additional presence of TiO_2 on AZT may actively enhance sulfur durability.

The purpose of this investigation is to improve the sulfur durability of NSR catalyst supports. In this investigation, the sulfur durability of AZT was verified, and the effect of titanium doping (TiO_2 onto AZT) on sulfur durability was examined.

2. Experimental

2.1. Preparation of supports

AZT was prepared by a conventional coprecipitation method [18]. The mole ratio of Al_2O_3:ZrO_2:TiO_2 was 50:30:20 (mol%).

Titanium-doped AZT (Ti–AZT) was synthesized by impregnation with titanium citrate [19]. AZT was added to an aqueous solution of titanium citrate and the solution was then evaporated at 373 K. The obtained product was then calcined at 1073 K for 5 h in air. The amount of doped Ti was 3.3 at.%, based on the metal atom composition of Ti–AZT (3.3 at.% Ti–AZT). 3.3 at.% Ti–AZT was used as the standard sample for all experiments. The final mole ratio of Al_2O_3:ZrO_2:TiO_2 was 48.3:28.0:23.7 (mol%). To clarify the dependency of the structural change on the amount of titanium added, Ti–AZT with 1.6 and 6.2 at.% of doped titanium (1.6/6.2 at.% Ti–AZT, respectively) were also synthesized as reference samples.

Pure γ-Al_2O_3 was prepared by the same method as that used for AZT. Pure ZrO_2–TiO_2 was prepared by the same method, as reported in literature [6]. A reference support was obtained by physically mixing pure γ-Al_2O_3 and ZrO_2–TiO_2 (physically mixed oxide). The composition of the physically mixed oxide was the same as that of AZT.

2.2. Characterization of Ti–AZT

The crystal structures were characterized by powder X-ray diffraction (XRD). XRD patterns were recorded using a Rigaku RINT-2100 (Cu Kα radiation λ = 1.5418 Å, 40 kV, 30 mA). To analyze the distribution of doped titanium and the composition of Al, Zr and Ti, field-emission-transmission electron microscopy (FE-TEM) and energy dispersive X-ray analysis (EDX) were performed using a Hitachi HF-2000. The diameter of the EDX analysis area was approximately 1 nm. The Brunauer–Emmett–Teller (BET) surface area was measured by N_2 adsorption at 77 K using a Micro Data, Micro Sorp 4232II. The pore size distribution was calculated from the intrusion curve obtained by mercury porosimetry using a Quantachrome Pore Master GT60-1.

The surface base properties of the supports were measured by CO_2-temperature programmed desorption (CO_2-TPD). Samples were formed into 0.3–0.7 mm diameter pellets. For CO_2-TPD, samples were pretreated at 773 K under a He atmosphere. After the samples were exposed to CO_2 in a stream of He at 373 K, they were heated to 773 K at a rate of 20 K/min. CO_2 desorbed from samples under a N_2 atmosphere was observed using a non-dispersive infrared (NDIR) analyzer attached to a Horiba MEXA-7100 exhaust gas evaluation system.

To investigate the thermal stability, samples were heated at 1073, 1173 and 1273 K for 5 h in air containing 3% water. The crystal structure after this thermal treatment was then analyzed using XRD and the particle size of ZrO_2–TiO_2 was calculated using Scherrer's formula [20]. The peak at $2\theta = 30.4^\circ$, assigned to the tetragonal ZrO_2 (1 0 1) phase, was used to calculate the particle size of ZrO_2–TiO_2. The BET surface area was also measured at each thermal treatment temperature by N_2 adsorption at 77 K using a Micro Data, Micro Sorp 4232II.

2.3. Sulfur desorption test

Catalysts were prepared by impregnating $Pt(NH_3)_2(NO_2)_2$ and $Rh(NO_3)_3$ (Tanaka Precious Metals), then dried at 383 K for 12 h, and finally calcined at 523 K for 3 h in air. The amount of Pt and Rh loading was 1.23 and 0.06 wt%, respectively. The powder obtained was then added to an aqueous solution containing $(CH_3COO)_2Ba$ and CH_3COOK (Wako Pure Chemical Industries) as precursors to the storage materials. The amounts of Ba (BaO) and K (K_2O) loadings were 18.8 and 5.8 wt%, respectively. After the catalysts were dried at 383 K for 12 h, they were calcined at 773 K for 3 h in air. The powder obtained was formed into 0.3–0.7 mm diameter pellets.

For the sulfur desorption tests at fixed temperature, catalysts were exposed to the SO_2 adsorption gas atmosphere (Table 1) for 30 min at 823, 873 and 923 K. After the condition was switched to the SO_2 desorption gas atmosphere, the sulfur species desorbed from the catalysts were measured using a Best Sokki Bex-5900 with a flame photometric detector (FPD) at fixed temperature.

For SO_2-TPD, catalysts were exposed to a SO_2 adsorption gas atmosphere (Table 1) at 873 K for 30 min. After the samples were cooled to 373 K, they were heated to 1023 K at a rate of 15 K/min under the SO_2 desorption gas atmosphere. The sulfur species desorbed from catalysts were measured using a FPD.

Table 1
Gas composition for sulfur desorption test at fixed temperature, SO_2-TPD, and NO_x storage measurement

Atmosphere	C_3H_6 (%C)	CO (%)	H_2 (%)	NO (ppm)	CO_2 (%)	SO_2 (ppm)	O_2 (%)	H_2O (%)
Sulfur desorption test and SO_2-TPD[a]								
SO_2 adsorption	0	0	0	0	0	400	6.6	3
SO_2 desorption	0.34	5.6	1.9	50	11	0	0	3
NO_x storage measurement[b]								
Lean	0.02	0	0	800	11	0	6.6	3
Rich	0.11	5.6	1.9	0	11	0	0.3	3
Rich spike	0.11	5.6	1.9	50	11	0	0	3

[a] N_2 balance.
[b] He balance.

Table 2
Ti/Zr/Al composition on Al_2O_3 primary particles of AZT and Ti–AZT observed in EDX analysis

	Composition (at.%)		
	Ti	Zr	Al
AZT			
Spot 1	1.6	0	98.4
Spot 2	4.0	2.5	93.5
Spot 3	3.8	2.4	93.8
Ti–AZT			
Spot 1	11.6	1.6	86.8
Spot 2	11.5	1.8	86.7
Spot 3	12.6	3.7	83.7

Both desorption experiments detailed above were performed under the same gas conditions. The gas flow rate was 4000 cm^3/min for the adsorption step and 3000 cm^3/min for the desorption step. The gas hourly space velocities (GHSV) were 240,000 and 180,000 h^{-1} for the adsorption and desorption steps, respectively. The mole ratio of SO_2 to the storage materials was S/(Ba + 0.5K) = 1.4. All the SO_2 was adsorbed on the catalysts under these conditions.

The residual amount of sulfur deposit in the SO_2-aged catalysts was measured using a combustion infrared absorption analyzer (Horiba EMIA-1200). The SO_2-aged sample was prepared at 873 K by switching the lean and rich gas atmospheres (Table 1) every 30 s with 1000 ppm SO_2. The mole ratio of SO_2 to the storage materials was S/(Ba + 0.5K) = 1.5.

2.4. NO_x storage measurement after the sulfur aging test

Catalysts were prepared in the same manner as the method given in Section 2.3. The sulfur aging test was carried out at 873 K under the SO_2 adsorption gas atmosphere shown in Table 1. The gas flow rate was 4000 cm^3/min and the GHSV was 240,000 h^{-1}. The mole ratio of SO_2 to storage materials was S/(Ba + 0.5K) = 1.4.

The amount of NO_x stored in the sulfur-aged catalysts was measured using a conventional fixed-bed flow reactor system at atmospheric pressure. Table 1 shows the composition of the feedstreams used to simulate actual engine exhaust gases for this measurement. After the catalyst was exposed to a rich atmosphere at 873 K for 5 min as the pretreatment, the catalyst was cooled to 573 K under the rich atmosphere. The gas was switched to the lean atmosphere until the outlet NO_x concentration reached a constant value, and then a 3 s rich spike was introduced to the catalyst. Subsequently, the gas was switched to the lean atmosphere until the outlet NO_x concentration reached a constant value. The amount of NO_x stored was calculated as the difference in the NO_x amount between the inlet and the outlet gases after the rich spike.

The amounts of NO_x stored at 673 and 773 K were measured in the same manner as for 573 K, and these measurements were carried sequentially after the experiment at 573 K. The gas flow rate was 3000 cm^3/min and the GHSV was 180,000 h^{-1}. The NO_x concentration was measured using a chemiluminescence NO_x meter attached to a Horiba MEXA-7100 gas exhaust evaluation system.

3. Results and discussion

3.1. Effect of AZT on sulfur desorption

3.1.1. EDX analysis of titanium on Al_2O_3 in AZT

AZT has low basicity [18]; therefore, it may be inferred that this low basicity results from the presence of a small amount of TiO_2 on Al_2O_3, because TiO_2 has high acidity/low basicity. To confirm this, EDX analysis of an Al_2O_3 primary particle in AZT was carried out.

The compositions shown in Table 2 are from three selected analysis spots of randomly sampled Al_2O_3 primary particles. Ti was observed in all the analysis spots. Zr was also detected in several spots, but the amount of Zr was smaller than that of Ti. The original Zr concentration in AZT was larger than the Ti concentration. Therefore, small amounts of Ti tend to be present in the Al_2O_3 primary particles, due to the coprecipitation synthesis step. Ti is thought to be present as an Al_2O_3–TiO_2 solid solution, because discrete TiO_2 particles were not observed on the Al_2O_3 particles by TEM and XRD examination [18]. Furthermore, a small amount of TiO_2 is soluble in Al_2O_3 [21,22].

This support structure suggests that it is possible to inhibit the adsorption of SO_x onto the surface. The desorption of sulfur compounds will be also easily promoted under a rich condition after SO_x adsorption onto the surface [23].

3.1.2. Sulfur desorption test

In practical use, the NSR catalyst is exposed to SO_2. To confirm the effect of the presence of TiO_2 in Al_2O_3 on the sulfur durability, the desorption of sulfur from catalysts was observed at a fixed temperature. Fig. 2 shows the amounts of sulfur desorption at each measured temperature. For all temperatures, the AZT catalyst had a larger amount of sulfur desorption than the catalyst containing the physically mixed oxide. In particular, AZT showed a larger amount of sulfur desorption at less than 873 K. The sulfur desorption at less than 873 K mainly corresponds to desorption from the surface of the support [7]. Therefore, SO_2 adsorbed onto

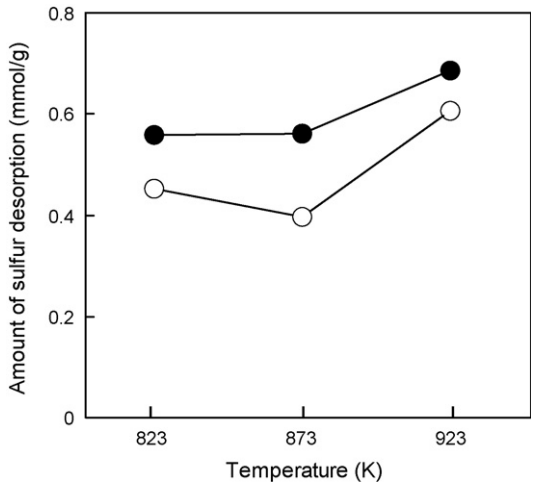

Fig. 2. Amount of sulfur desorption from NSR catalysts at a fixed temperature. (●) AZT catalyst; (○) physically mixed catalyst.

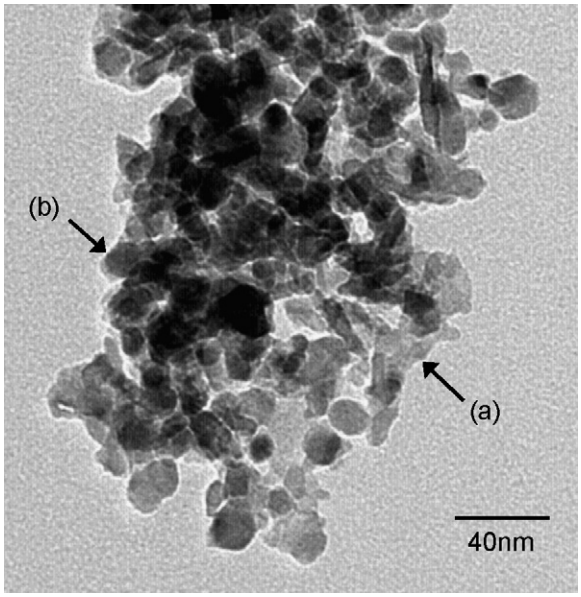

Fig. 3. FE-TEM micrograph of 3.3 at.% Ti–AZT. Arrows (a) and (b) indicate examples of an Al_2O_3 primary particle and a ZrO_2–TiO_2 primary particle, respectively.

the AZT catalyst is easily desorbed at low temperature, because of the lower basicity as the effect of the presence of TiO_2 on the Al_2O_3 surface emerges.

On the basis of this result, Ti–AZT was conceptualized and synthesized in order to enhance the total sulfur durability.

3.2. Characterization of Ti–AZT

3.2.1. Analysis of the structure and the composition by TEM and EDX

Fig. 3 shows a TEM image of the 3.3 at.% Ti–AZT sample. The structure of Ti–AZT is the same as that of AZT [18]. Al_2O_3 primary particles (amorphous-shape particles) and ZrO_2–TiO_2 primary particles (distinct-shape particles) also coexisted in the same secondary particles. No discrete TiO_2 particles were observed in Ti–AZT. This indicates that Ti is present homogeneously on the AZT surface and may be dissolved in the Al_2O_3 phase as an Al_2O_3–TiO_2 solid solution. TiO_2 is simultaneously dissolved in the ZrO_2–TiO_2 solid solution, because the synthesis method involved the impregnation of AZT with the Ti salt solution.

In order to clarify the Ti concentration on the Al_2O_3 particles, random analysis spots of Al_2O_3 primary particles were examined using EDX. The compositions of three selected spots are listed in Table 2. The Ti concentration was more than 10 at.% in each analysis spot, although the amount of Ti doped was 3.3 at.%. Therefore, the surface of the Al_2O_3 particle was modified with Ti in a dispersed state, and this surface localization is expected to work effectively for sulfur resistance.

3.2.2. Analysis of the structure by XRD

In order to confirm the presence of discrete TiO_2 particles and analyze the crystal structure, XRD patterns of Ti–AZT with different Ti amounts were measured, and are shown in Fig. 4. AZT has the γ-Al_2O_3 phase and tetragonal ZrO_2 phase with a peak shift at the (1 0 1) peak due to the formation of the ZrO_2–TiO_2 solid solution [18]. All of the Ti–AZT samples contained the same AZT structure. Although the doped Ti is thought to be present on both ZrO_2–TiO_2 and γ-Al_2O_3, further shift of the (1 0 1) diffraction peak for the tetragonal ZrO_2 phase was not observed. This is because the amount of Ti doped in the ZrO_2–TiO_2 is too small to observe further peak shift.

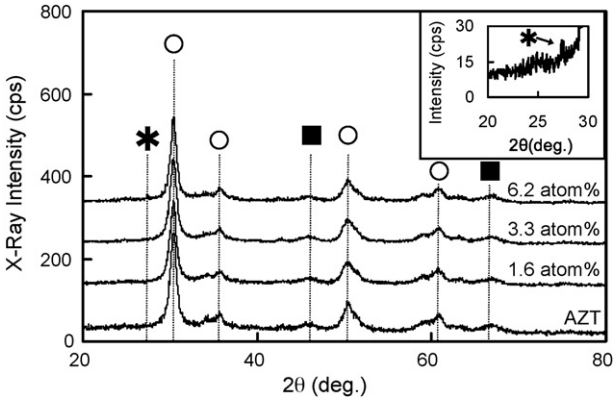

Fig. 4. XRD patterns of Ti–AZT with various amounts of Ti doping. The inset shows an enlarged view of 6.2 at.% Ti–AZT around the rutile-TiO_2 (1 0 0) peak. (○) Tetragonal ZrO_2; (■) γ-Al_2O_3; (✱) rutile-TiO_2.

The 1.6 and 3.3 at.% Ti–AZT samples revealed no crystalline TiO_2 phase. This indicates that doped Ti is present on the surface of both the Al_2O_3 particles, as an Al_2O_3–TiO_2 solid solution, and ZrO_2–TiO_2 solid solution particles. On the other hand, 6.2 at.% Ti–AZT revealed a crystalline rutile TiO_2 peak. It has been reported that the formation of an Al_2O_3–TiO_2 solid solution depends on the amount of doped Ti [21,22]. Therefore, the excess amount of Ti in 6.2 at.% Ti–AZT is considered to form discrete rutile TiO_2 particles. TiO_2 particles have weak thermal stability and cause poor catalytic performance after thermal aging, because TiO_2 easily aggregates and reacts with the NO_x storage materials [6]. In this system, it is better to maintain the doped titanium amount at less than 3.3 at.% for the support of a NSR catalyst; therefore, 3.3 at.% Ti–AZT was used as the standard sample in the subsequent experiments.

3.2.3. Base property

Table 3 shows the amount of base determined by CO_2-TPD. Although the CO_2 desorption of Ti–AZT was found at the same temperature region as that for AZT, the maximum CO_2 concentration of Ti–AZT was small compared with that of AZT. The amount of base in Ti–AZT was reduced by 25% relative to that in AZT, and by more than 80% relative to that of the physically mixed oxide, which has 12.1 μmol/g of base [18]. The amount of base is in good inverse proportion to the amount of Ti on Al_2O_3. Therefore, the basicity of Al_2O_3 is canceled by the acidic TiO_2, and the increased presence of TiO_2 is effective in further lessening the affinity of the catalyst support with acidic gases.

3.2.4. Surface area and pore distribution

Table 3 shows the specific surface area (SSA) of Ti–AZT and AZT. Ti–AZT maintained a high SSA, although it was slightly decreased compared with AZT. From the results of TEM and XRD, it was determined that this slight drop in SSA results not from discrete TiO_2 particles, but from the formation of a TiO_2–Al_2O_3 solid solution [21].

Fig. 5 shows the pore diameter distribution, and Table 3 lists the mesopore volume of each sample. Ti–AZT had a single sharp mesopore peak around 15 nm (Fig. 5, black line) and almost the same mesopore volume as AZT. These results indicate that the

Table 3
Base amount, surface area, and mesopore volume

	Base amount (μmol/g)	SSA (m^2/g)	Mesopore volume (cm^3/g)
AZT	2.7	128	0.41
Ti–AZT	2.1	112	0.39

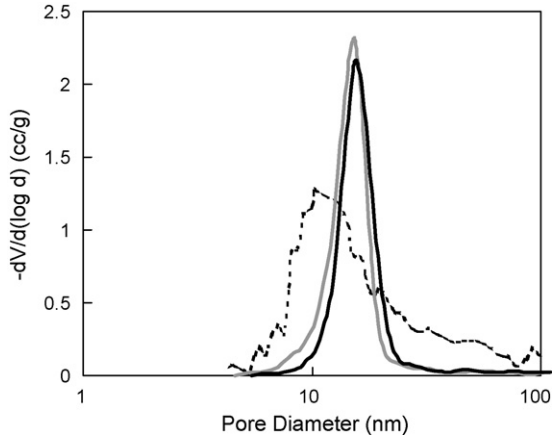

Fig. 5. Pore distribution of samples. Ti–AZT (—); AZT (▬); physically mixed Al_2O_3 and ZrO_2–TiO_2 (- - -).

morphology of the original AZT structure was maintained after the Ti doping step.

3.2.5. Thermal stability

To confirm the thermal stability of Ti–AZT, the particle size of ZrO_2–TiO_2 after thermal treatment was investigated by XRD, based on the ZrO_2 (1 0 1) peak data. Fig. 6 shows the average particle size of ZrO_2–TiO_2 at each thermal treatment temperature. The particle size of ZrO_2–TiO_2 in Ti–AZT was almost identical to that in AZT at each temperature. The SSA for each thermal treatment temperature showed that Ti–AZT has the same SSA variation as AZT, as shown in Fig. 7.

As previously shown, the morphology of AZT is maintained through the Ti doping step; therefore, Ti–AZT has the same thermal stability as AZT, and is expected to exhibit high NO_x storage performance with not only sulfur durability, but also thermal stability.

3.3. Catalytic application of Ti–AZT

3.3.1. SO_2-TPD

The inhibition of SO_x adsorption and the promotion of sulfur species desorption are required to improve the sulfur durability of NSR catalysts. Fig. 8 shows the SO_2-TPD spectra for the catalysts

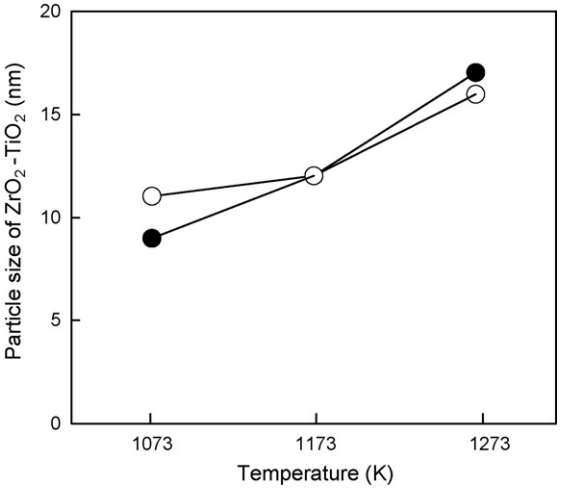

Fig. 6. Average particle size of ZrO_2–TiO_2 determined by XRD data as a function of thermal treatment temperature. (●) Ti–AZT; (○) AZT.

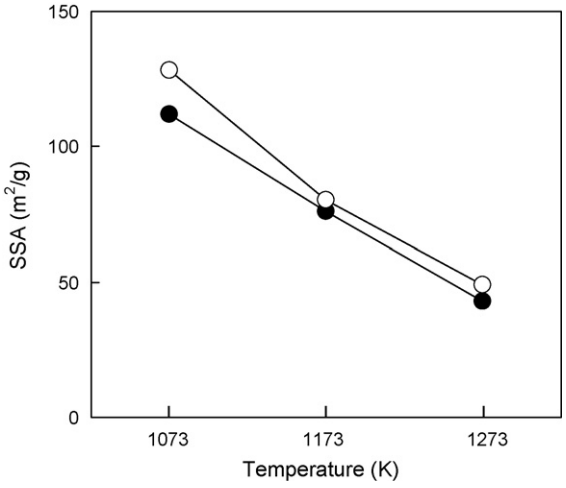

Fig. 7. SSA of samples as a function of thermal treatment temperature. (●) Ti–AZT; (○) AZT.

from 623 to 1023 K. The Ti–AZT catalyst has a larger amount of sulfur desorption at low temperature around 750 K than the AZT catalyst. In addition, the starting temperature of sulfur desorption from the Ti–AZT catalyst is 700 K, which is approximately 20 K lower temperature than that for the AZT catalyst. Sulfur species desorb from γ-Al_2O_3 surfaces at less than 873 K [7]; therefore, it was determined that the Ti–AZT catalyst facilitates sulfur desorption from the support. In addition, the starting temperature of sulfur desorption from Ti–AZT is decreased, in accordance with the Ti doping concept.

Furthermore, the sulfur concentration of the Ti–AZT catalyst was low from 823 to 980 K, although both catalysts had the same sulfur concentration at around 1000 K. It has been understood that desorbed sulfur species are derived from the decomposition of barium sulfate at more than 873 K in the Pt/Ba/γ-Al_2O_3 system [7]. Therefore, there is a possibility that the amount of sulfate materials in the Ti–AZT catalyst is smaller than that in the AZT catalyst. To confirm this, the amount of residual sulfur deposit was examined following the SO_2 aging test at 873 K. As a result, the SO_2-aged Ti–AZT catalyst had 2.5 wt% of residual sulfur deposit, and the AZT catalyst had 2.8 wt%. This indicates that the amount of sulfur derived from sulfur poisoned NO_x storage materials is small in the Ti–AZT catalyst. Therefore, a close relationship between the following two kinds of sulfur poisoning is suggested: sulfur coverage resulting in SO_x adsorption on catalysts and sulfate

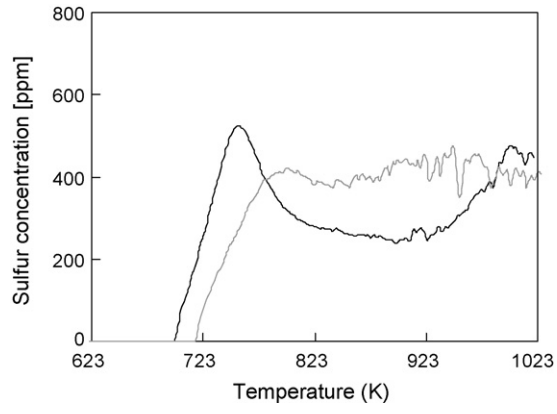

Fig. 8. Sulfur desorption spectra of samples. Ti–AZT catalyst (—); AZT catalyst (▬).

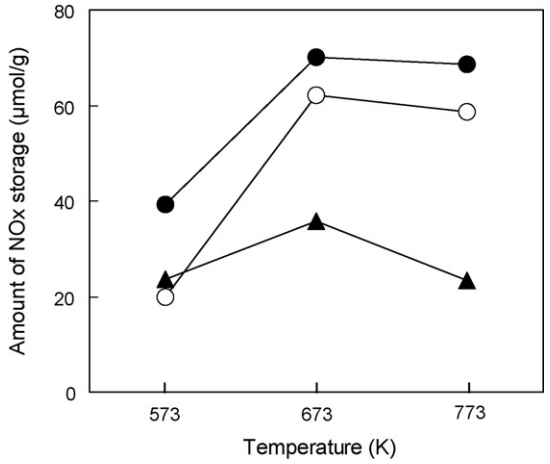

Fig. 9. NO_x storage performance after sulfur aging tests as a function of the reaction temperature. (●) Ti–AZT catalyst; (○) AZT catalyst; (▲) physically mixed catalyst.

formation of NO_x storage materials. The inhibition of SO_x adsorption may introduce the inhibition of sulfate formation of neighboring NO_x storage materials, considering that the main improvement in this novel support is the lowered basicity. Clarification of the detailed relationship should be carried out in the future; however, this attribute is expected to lead to NSR catalysts with higher performance for NO_x storage.

3.3.2. NO_x storage performance

To verify the effect of the Ti–AZT catalyst on sulfur durability as a NSR catalyst, the NO_x storage of the catalysts was measured after the sulfur aging test. These catalysts were pretreated at 873 K under a rich gas condition before the NO_x storage measurements.

Fig. 9 shows the amount of NO_x storage at each temperature. The Ti–AZT catalyst has a larger amount of NO_x storage than the AZT catalyst. This difference results from the reduction in not only the affinity of the catalyst surface with SO_2, but also in the amount of sulfur poisoned NO_x storage materials, as mentioned in Section 3.3.1. The active Ba and K NO_x storage species are assumed to form nitrate species such as $Ba(NO_3)_2$ and KNO_3 under lean conditions, as reported in the literature [5,24,25].

NSR catalysts continuously suffer from SO_x poisoning, as well as thermal deterioration, in the presence of actual exhaust gases from lean-burn engines. Ti–AZT has acquired sulfur durability in addition to the thermally stability characteristics of the original AZT support. Therefore, Ti–AZT is an ideal material for practical use as a NSR catalyst support.

4. Conclusion

Ti–AZT was synthesized as a support for NSR catalyst based on AZT. All Al_2O_3 primary particles in Ti–AZT had higher Ti concentrations than those in AZT. Ti–AZT maintains the original AZT structure with thermal stability after Ti doping, and provides a support with low basicity.

From the SO_2-TPD results, the Ti–AZT catalyst promotes significant sulfur desorption relative to the AZT catalyst. After sulfur aging tests, the Ti–AZT catalyst had a larger amount of NO_x storage than the AZT catalyst.

The improved sulfur durability of this NSR catalyst has resulted from the doping of Ti as an Al_2O_3–TiO_2 solid solution in AZT. Therefore, Ti–AZT has acquired sulfur durability and maintained the thermal stability of the original AZT support, thereby meeting the requirements for NSR catalysts.

References

[1] S. Sato, Y. Yu-u, H. Yahiro, N. Mizuno, M. Iwamoto, Appl. Catal. 70 (1991) L1.
[2] Y. Kintaichi, H. Hamada, M. Tabata, M. Sasaki, T. Ito, Catal. Lett. 6 (1990) 239.
[3] R. Burch, P.J. Millington, Catal. Today 26 (1995) 185.
[4] W. Bögner, M. Krämer, B. Krutzsch, S. Pischinger, D. Voigtländer, G. Wenninger, F. Wirbeleit, M.S. Brogan, R.J. Brisley, D.E. Webster, Appl. Catal. B: Environ. 7 (1995) 153.
[5] N. Takahashi, H. Shinjoh, T. Iijima, T. Suzuki, K. Yamazaki, K. Yokota, H. Suzuki, N. Miyoshi, S. Matsumoto, T. Tanizawa, T. Tanaka, S. Tateishi, K. Kasahara, Catal. Today 27 (1996) 63.
[6] N. Takahashi, A. Suda, I. Hachisuka, M. Sugiura, H. Sobukawa, H. Shinjoh, Appl. Catal. B: Environ. 72 (2006) 187.
[7] S. Matsumoto, Y. Ikeda, H. Suzuki, M. Ogai, N. Miyoshi, Appl. Catal. B: Environ. 25 (2000) 115.
[8] E.C. Corbos, X. Courtoins, N. Bion, P. Marecot, D. Duprez, Appl. Catal. B: Environ. 80 (2008) 62.
[9] X. Wei, X. Liu, M. Deeba, Appl. Catal. B: Environ. 58 (2005) 41.
[10] J. Dawody, M. Skoglundh, L. Olsson, E. Fridel, Appl. Catal. B: Environ. 70 (2007) 179.
[11] Z. Liu, J. Anderson, J. Catal. 228 (2004) 243.
[12] K. Yamamoto, R. Kikuchi, T. Takeguchi, K. Eguchi, J. Catal. 238 (2006) 449.
[13] T. Kanazawa, Catal. Today 96 (2004) 171.
[14] K. Ito, S. Kakino, K. Ikeue, M. Machida, Appl. Catal. B: Environ. 74 (2007) 137.
[15] K.M. Adams, G.W. Graham, Appl. Catal. B: Environ. 80 (2008) 343.
[16] M. Casapu, J. Grunwaldt, M. Maciejewski, M. Wittrock, U. Göbel, A. Baiker, Appl. Catal. B: Environ. 63 (2006) 232.
[17] N. Takahashi, S. Matsunaga, T. Tanaka, H. Sobukawa, H. Shinjoh, Appl. Catal. B: Environ. 77 (2007) 73.
[18] H. Imagawa, T. Tanaka, N. Takahashi, S. Matsunaga, A. Suda, H. Shinjoh, J. Catal. 251 (2007) 315.
[19] M. Milanova, M. Arnaudov, M. Getsova, D. Todorovsky, J. Alloys Compd. 264 (1998) 95.
[20] Y. Xie, C. Yuan, Appl. Catal. B: Environ. 46 (2003) 251.
[21] W. Zhaobin, X. Qin, G. Xiexian, Appl. Catal. 63 (1990) 305.
[22] L.O. Öhman, J. Paul, Mater. Chem. Phys. 73 (2002) 242.
[23] H.Y. Huang, R.Q. Long, R.T. Yang, Appl. Catal. B: Environ. 33 (2001) 127.
[24] M. Takeuchi, S. Matsumoto, Top. Catal. 28 (2004) 151.
[25] N. Takahashi, K. Yamazaki, H. Sobukawa, H. Shinjoh, J. Chem. Eng. Jpn. 39 (2006) 437.